Distributed Parameter Modeling and Control of Electromagnetic Molding Machine

Takayuki Ishizaki, Kenji Kashima, Jun-ichi Imura*, Atushi Katoh and Hiroshi Morita**

***Abstract*— In this paper, we propose a mathematical model for an electromagnet placed inside a molding machine and design a PI controller for this system. The eddy currents inside the electromagnet are a spatially-distributed phenomenon that is difficult to capture by using finite-dimensional systems. First, based on an expression of the system as partial differential equations, we analyze essential properties of the system. From the analysis, we derive a suitable model for a control system design in the frequency domain. Second, we propose a new loop shaping technique that utilizes GKYP lemma for this system.**

I. INTRODUCTION

In molding fabrication, machines which generate mold clamping forces are called molding machines. In the past, molding machines driven by oil pressure were dominant. Recently, electric molding machines are widely used to improve controllability and cycling time of jobs. Furthermore, electromagnetic molding machines, driven by electromagnets, are currently proposed [1]. In the machines, a suction force generated by the electromagnets is directly transmitted to a mold in contrast to general electric molding machines, in which a thrust force generated by a rotary motor is transmitted through amplification. As a consequence, the electromagnetic molding machines are capable of more precise molding fabrication.

However, it is difficult to realize desired force responses using heuristic tunings of controllers. The reason is that eddy currents are spatially distributed in an iron core of the electromagnet. This means that the system should be treated as a distributed parameter system [6], [12], [13], [15]. Therefore, the system is difficult to model in finite dimensions while keeping suitable properties for control system design.

To model the system, we first execute the spatial discretization of partial differential equations (PDEs) [10], which are derived from basic laws of physics and perfectly represent the behavior of the system. However, it will become clear that we cannot design an actual controller by only using the spatially-discretized models. This is because, they need a high order to represent the suitable properties of the system for the control system design. To derive a suitable model for the design, we examine the essential properties of the physical system by analytically characterizing input-output properties in the frequency domain. Finally, we design a PI controller for the model by loop shaping via GKYP lemma. In this paper, we restrict the structure of the controller to PI controllers for industrial applications.

This paper is organized as follows. In section II, we explain the features of an electromagnetic molding machine and the difficulty of the control system design using heuristic tuning. Furthermore, we derive the expression of the system as PDEs and analytically characterize the structure of the system in the frequency domain. In section III, we derive the spatially-discretized model and show by experiments that the model cannot represent suitable properties for the control system design using the model of practically low order. In section IV, we derive new models in the frequency domain from the expression of the system as PDEs. Then, we propose a new loop shaping technique to design the PI control system via GKYP lemma. Finally, we verify the validity of the proposed technique through experiments on the actual machine.

II. ELECTROMAGNETIC MOLDING MACHINE

A. Tuning of PI control system

Fig. 1 shows electromagnets placed inside the molding machine. The electromagnets consist of an *electromagnet core* and a *coil*. They generate magnetic flux, shown in Fig. 1, by the current flowing in the coil. Sucking forces are generated by the magnetic flux at *gaps* in the electromagnet core. They are transmitted to the mold of the machine.

To control the electromagnetic molding machine, the responses of the molding force need to settle in a short time without overshoot. Fig. 2 shows a block diagram of the PI control system. In this figure, the electromagnets, shown in Fig. 1, are represented by the electro magnet block. The filter, which has a low-pass property, expresses a certain time delay included in the actual machine (See section III-C for detail).

Fig. 3 shows experimental results of the step response of the molding force[1] when we vary a proportional gain of the control system. Generally, the convergent rate to a target value is larger as the proportional gain of PI control systems is enlarged and when the gain reaches some threshold, the overshoots of the response will arise. However, in the case of the electromagnetic molding machine, we can see from Fig. 3 that the convergent rate does not increase even if the gain is enlarged.

From these experiments, we can see that the behavior of this machine contradicts the intuition of general systems. Therefore, it can be anticipated that the performance of the machine will be hard to improve with the traditional tuning

*Graduate School of Information Science and Engineering, Tokyo Institute of Technology; 2-12-1, Meguro ward, Tokyo {ishizaki,kashima,imura}@cyb.mei.titech.ac.jp

**Sumitomo Heavy Industries, Ltd; 19, Natushima, Yokosuka city, Kanagawa {Ats_Katoh,hrh_morita}@shi.co.jp

[1]In this paper, the sampling times of the experiment were set at 1.5kHz.

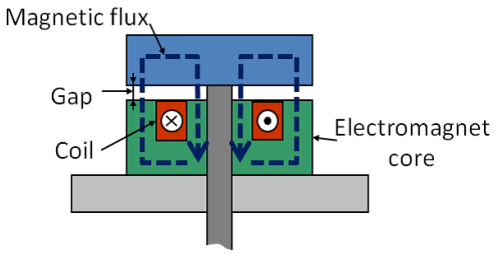

Fig. 1. Electromagnet system

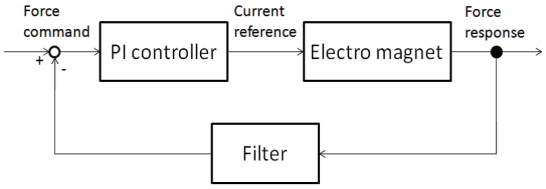

Fig. 2. PI control system

techniques of controllers [2]. To design the control system systematically, we first derive the mathematical expression of the system.

B. System expression as partial differential equations

The physical system is supposed to be axisymmetric as shown in Fig. 4, in which r, $B(t,r)$ and $i_c(t)$ denote the spatial variable for the radial direction, the density of the magnetic flux and the current in the coil, respectively. Because of the symmetry, it suffices to model the system only for the radial direction. Here, we define the state variable and the input of the system by $\chi(t,r) := B(t,r)$ and $\upsilon(t) := i_c(t)$. Furthermore, we define the output $\Upsilon(t)$ by a suction force generated by the magnetic flux and then linearize the output around an operating point $(\overline{\upsilon}, \overline{\chi}, \overline{\Upsilon})$. Now transforming the spatial coordinate as $r = \sqrt{\xi}$ for convenience, we obtain

$$\begin{cases} \dfrac{\partial \hat{\chi}(t,\xi)}{\partial t} = 2\alpha \dfrac{\partial}{\partial \xi}\left(\xi \dfrac{\partial \hat{\chi}(t,\xi)}{\partial \xi}\right) & \text{at} \quad \xi \in (0,1) \\ \hat{\chi}(t,\xi) = \dfrac{\beta}{\alpha}\upsilon(t) & \text{at} \quad \xi = 1 \\ \xi \dfrac{\partial \hat{\chi}(t,\xi)}{\partial \xi} = 0 & \text{at} \quad \xi = 0 \\ \Upsilon(t) = \displaystyle\int_0^1 \hat{\chi}(t,\xi)\, d\xi, \end{cases} \tag{1}$$

where $\hat{\chi}(t,\xi) := \chi\left(t, \sqrt{\xi}\right)$, and $\alpha, \beta \in \mathbb{R}$ are positive constants. Therefore, the dynamics of the physical system are essentially identical to that of heat diffusion systems with a diffusivity which is proportional to the spatial variable [12], [13], [14]. Next, we characterize the input-output properties of the system in the frequency domain.

Theorem 1: The transfer function of the system expressed in (1) is given by

$$G_\infty(s) := \frac{\beta}{\alpha} \frac{J_1\left(2\sqrt{-\frac{s}{2\alpha}}\right)}{\sqrt{-\frac{s}{2\alpha}} J_0\left(2\sqrt{-\frac{s}{2\alpha}}\right)}, \tag{2}$$

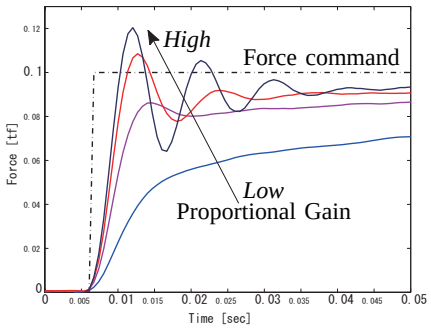

Fig. 3. Step response of electromagnet system

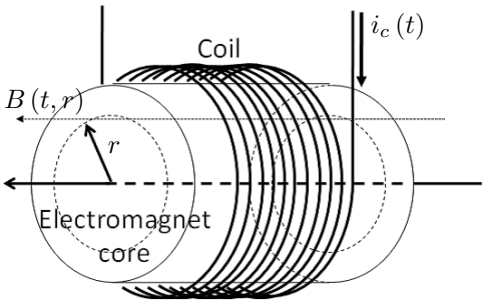

Fig. 4. Model of electromagnet

where

$$J_k(z) = \sum_{m=0}^{\infty} \frac{(-1)^m}{m!\,(m+k)!} \left(\frac{z}{2}\right)^{2m+k} \tag{3}$$

are Bessel functions.

Theorem 2: The transfer function $G_\infty(s)$ defined by (2) satisfies the following conditions:

(i) $G_\infty(s)$ is H^∞ function expressed as the ratio of entire functions.

(ii) The zeros and poles of $G_\infty(s)$ are all negative real numbers. The zeros and poles alternate as we traverse the real axis from 0 to $-\infty$.

(iii) A high- and low-frequency properties of $G_\infty(s)$ are respectively given by

$$\begin{cases} G_\infty(0) = \dfrac{\beta}{\alpha} \\ G_\infty(j\omega) \sim \dfrac{\beta}{\alpha}\sqrt{\dfrac{2\alpha}{j\omega}}, \quad \omega \gg 1. \end{cases}$$

See section III-A for the physical interpretation of Theorems 1 and 2. (The proofs of these are omitted by the convenience of the wide of the paper.)

III. Derivation of Spatially-Discretized Model and Control System Design

A. Spatially-discretized model

By discretizing (1) with respect to the spatial variable ξ [10], we obtain a finite-dimensional approximated system

expressed as

$$\begin{cases} \dot{x} = Ax + Bu \\ y = Cx \end{cases} \tag{4}$$

$$\begin{aligned} A &:= -\alpha N D^{-\mathsf{T}} R D^{-1} \in \mathbb{R}^{N\times N} \\ B &:= \beta N r_N \left[1, 0, \cdots, 0\right]^{\mathsf{T}} \in \mathbb{R}^{N\times 1} \\ C &:= \frac{1}{N}[1 \ \cdots \ 1] \in \mathbb{R}^{1\times N}, \end{aligned} \tag{5}$$

where N denotes the approximated order and

$$D := \begin{bmatrix} 1 & & \\ \vdots & \ddots & \\ 1 & \cdots & 1 \end{bmatrix} \in \mathbb{R}^{N\times N} \tag{6}$$

$$R := \mathrm{diag}\left\{r_N, \cdots, r_1\right\} \in \mathbb{R}^{N\times N} \tag{7}$$

$$r_n = 2n. \tag{8}$$

Furthermore, we denote the transfer function of this system as

$$G_N(s) := C(sI - A)^{-1}B. \tag{9}$$

This model is physically reasonable since the stability and the steady-state value of the step response do not vary with the order N.

Next, we explain variations of the frequency property of the spatially-discretized model $G_N(s)$ when varying the order N. Fig. 5 shows the Bode diagrams of $G_N(s)$ $(N = 1, 10, 40, 80)$ and $G_\infty(s)$. From this figure, we can see that the slope of the gain characteristic of the high-order model approaches to -10 [dB/dec] and the frequency response of $G_N(s)$ approaches to that of $G_\infty(s)$, shown in Theorem 1, for all frequencies.

From this tendency and Theorem 2 (i), we can expect that the behavior of $G_N(s)$ will come closer to that of the actual machine by increasing the order of $G_N(s)$. Furthermore, the fact that the zeros and poles of $G_\infty(s)$ exist alternately, as shown in Theorem 2 (ii), causes the gain to fall off at -10 [dB/dec]. This property is mathematically interpreted in Theorem 2 (iii).

B. Comparison with the experimental results on the actual machine

In this section, in order to verify the validity of the spatially-discretized model of first or higher order, we compare them with the experimental results on the actual machine [4].

Fig.6 shows Bode diagrams of the experimental results and the models. We can see from this figure that the slope of the gain characteristic of the actual machine is -10 [dB/dec] at high-frequency[2]. This feature conforms to that of the high-order model as explained in III-A. Furthermore, Fig. 7 shows the step responses of the PI control system, constructed in Fig. 2. We can see from this figure that the behavior of the high-order spatially-discretized model conforms to that of the experimental result.

[2]The mismatch of the phase at high-frequency might be caused from certain elements of the time delay included in the actual machine.

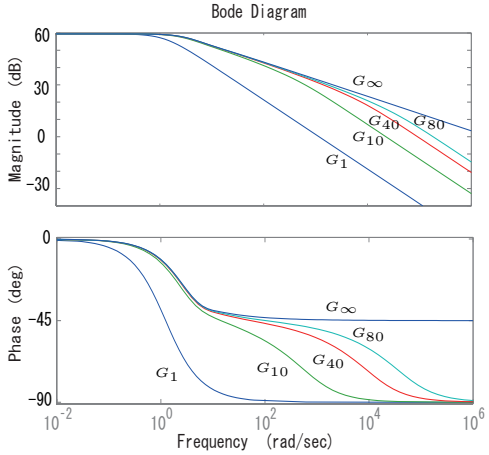

Fig. 5. Bode diagram of $G_\infty(s)$

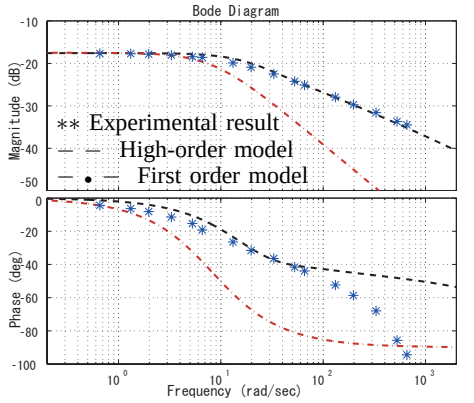

Fig. 6. Bode diagram of proposed electromagnet

Generally, the slope of the gain characteristic of systems with relative degree k is $-20k$ [dB/dec] at high-frequency. From this fact, we can anticipate that the property of the actual machine is hard to even approximately express in terms of a general lumped parameter system consisting of rational functions. Actually, as shown in Fig. 7, the first order model cannot represent the unique time response behavior of the actual machine.

Therefore, we conclude that only the spatially-discretized model of high-order can sufficiently represent the unique behavior of the actual machine.

C. PI control system design via GKYP lemma

In this section, we explain a design technique for the PI control system, shown in Fig. 2, via GKYP lemma [16]. In the rest of this paper, let the transfer function of the filter in Fig.2 be

$$F(s) = \left(\frac{1}{1+\tau s}\right)^2, \tau = 3.00 \times 10^{-4}. \tag{10}$$

This is given by means of identification experiments of the actual machine. Furthermore, we define the PI controller

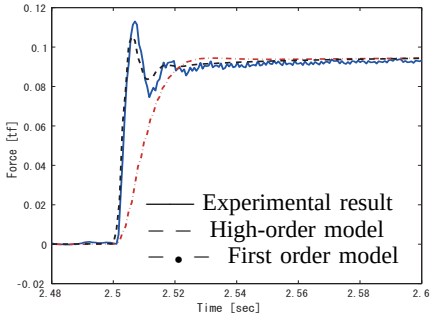

Fig. 7. Time responses of controlled system

$K(s)$ and the open-loop transfer function $L_\infty(s)$ of the system by

$$K(s) := k_{\rm P} + \frac{k_{\rm I}}{s} \tag{11}$$

$$L_\infty(s) := F(s)\,G_\infty(s)\,K(s). \tag{12}$$

The constants in (5) are given by $\alpha = 1.2352,\ \beta = 1.1621 \times 10^3$ to fit the properties of the actual machine.

In this paper, we design a control system based on frequency shaping of the open-loop transfer function. From the above discussion, we can expect to design a desired compensator by shaping L_∞ directly. However, there is no method to directly design an applicable compensator for distributed parameter systems [8], [9]. Therefore, we consider designing a compensator indirectly by applying GKYP lemma to our finite-dimensional approximated system.

Problem: Suppose that rational functions with complex coefficient $\tilde{P}_i(s)$, $\Omega_i \subset \mathbb{R}_+$ and $(a_i, b_i, c_i) \in \mathbb{R}^3$ for $i = 1, 2, \cdots, m$ are given. Find all $k_{\rm P}$ and $k_{\rm I}$ for which $L_i(s) := \tilde{P}_i(s)\,(k_{\rm P} + k_{\rm I}/s)$, $i = 1, 2, \cdots, m$ satisfy

$$a_i {\rm Re}\left[L_i(j\omega)\right] + b_i {\rm Im}\left[L_i(j\omega)\right] < c_i,\ \omega \in \Omega_i \tag{13}$$

for all i.

By applying GKYP lemma, this problem can be converted to LMIs, which we can efficiently solve by numerical computation. This is because, the structure of the controller is restricted to PI controllers [16], [17]. The physical interpretation of each sets and the parameters in this problem and relation to the actual design problem are explained throughout discussion in the next sections.

D. Loop shaping by using the spatially-discretized model

Intuitively, we can expect to design a desired PI controller by using $G_N(s)$ for a sufficiently large N. Here, we take $N = 5$ and then search for $k_{\rm P}$ and $k_{\rm I}$ so as to minimize κ under the constraints,

$$\begin{aligned}
&\tilde{P}_i(s) := F(s)\,G_5(s),\ i = 1, 2, 3\\
&\Omega_1 = [1, 5],\ (a_1, b_1, c_1) = (10, -1, 0)\\
&\Omega_2 = [500, 1100],\ (a_2, b_2, c_2) = (0, 1, -2)\\
&\Omega_3 = [2000, 8000],\ (a_3, b_3, c_3) = (-1.5, 1, \kappa).
\end{aligned}$$

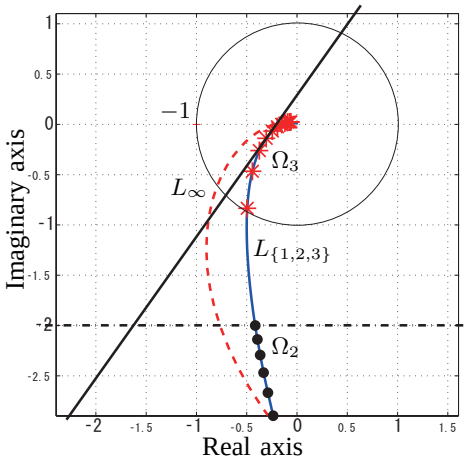

Fig. 8. Nyquist plot of the loop transfer functions

In this optimization problem, we minimize κ under the constraints of the half plane for the loop transfer function $\tilde{P}_i(s)$ in the frequency range Ω_i. The restriction boundaries are straight lines, which are defined by the parameters (a_i, b_i, c_i) $(i = 1, 2, 3)$. To put it concretely, the first and second restrictions guarantee some gains in the low- and middle-frequency range and the third restriction maximizes the stability margin by minimizing κ. Then, we search for $k_{\rm P}$ and $k_{\rm I}$ such that $L_i(s)$ satisfies these conditions. As a result, we obtained $k_{\rm P} = 0.0972,\ k_{\rm I} = 3.0121$ and $\kappa = 0.3283$.

Fig. 8 shows Nyquist plots of $L_{\{1,2,3\}}(s)$ and $L_\infty(s)$ when using the controller obtained here[3]. In this figure, : and $*$ denote the ranges Ω_2 and Ω_3, respectively. Looking at the Nyquist plots of $L_{\{1,2,3\}}(s)$, drawn by a solid line, we seem to guarantee the sufficiently large stability margin. However, according to the Nyquist plot of $L_\infty(s)$, drawn by a broken line, we can see that the stability margin of the closed-loop system decreases. The reason for making the stability margin smaller is that $G_5(s)$ cannot represent the frequency property of the system around the cut-off frequency of the filter, which is about 3000 [rad/sec]. That is to say, low-order models cannot sufficiently represent the frequency property around the cut-off frequency. From Fig. 5, we need to increase the order larger than about 80 in order to represent the frequency property of $G_\infty(s)$ around the cut-off frequency. However, we cannot solve the optimization problem for the 80th order model due to numerical problems caused by the considerable computational loads for solving LMIs.

IV. Derivation of new models in the frequency domain and control system design

A. Loop shaping by using the analytical expression of the transfer function

In this section, we propose a new loop shaping technique by using the high-frequency property of the system. In this technique, we execute the loop shaping for new models

[3]In the rest of paper, $L_1(s)$, $L_2(s)$ and $L_3(s)$ are collectively denoted by $L_{\{1,2,3\}}(s)$, for example.

which are restricted to a given frequency range, taken into special consideration in the loop shaping. Note that, when applying GKYP lemma, the general optimization problems are solved by imposing some restrictions on the *same* rational transfer functions with *real* coefficients, as similarly shown in section III-D. On the other hand, the proposed technique utilizes the following features of GKYP lemma: in GKYP lemma

- $\tilde{P}_i$ need not to equal $\tilde{P}_j$ for $i \neq j$.
- it is applicable even if $\tilde{P}_i$ is a rational transfer function with complex coefficients.

Hence, we can consider solving optimization problems by imposing some restrictions in each frequency range on *different* rational transfer functions with *complex* coefficients.

It is important that the model suitably represents the properties of the high-frequency range, which correspond to the cut-off frequency of the filter, in loop shaping. At the same time, the high-frequency properties of the system are given in Theorem 2 (iii). However, we cannot directly utilize Theorem 2 (iii) for designing the controller since the high-frequency properties in Theorem 2 (iii) are not the rational function.

Here, let $f(s;\omega_c,n)$ be the Taylor expansion of $f(s) := (1+\tau s)^2\sqrt{s}$ around a complex number $s = j\omega_c$ with an order n. If $\omega_c \gg 1$, we can approximately represent the high-frequency property by

$$\begin{aligned} F(s)\,G_\infty(s) &\sim \frac{\beta\sqrt{2\alpha}}{\alpha}\frac{1}{f(s;\omega_c,n)} \\ &=: P_{app}(s;\omega_c,n), \end{aligned} \tag{14}$$

a rational transfer function with complex coefficients. Using this approximation, we can execute loop shaping, restricted to given high-frequency ranges by directly applying GKYP lemma. Furthermore, we can expect to reduce some computational loads for solving LMIs since the approximation is not needed for all frequency ranges.

Fig. 9 shows Bode diagrams of $P_{app}(s;1000,3)$, $P_{app}(s;3000,3)$ and $F(s)\,G_\infty(s)$, drawn by a broken, chain and solid line, respectively. From this figure, we can confirm that the system is approximated sufficiently around the point of expansion. We can see that we can obtain the models which represent the suitable property for the loop shaping even $n = 3$. In addition, the sizes of the matrix are determined by the truncated order n, therefore we can reduce the computational loads for solving LMIs.

Next, we minimize κ under the constraints that $k_{\rm P}$ and $k_{\rm I}$ satisfy

$$\begin{aligned} &\tilde{P}_1(s) := F(s)\,G_5(s) \\ &\tilde{P}_2(s) := P_{app}(s;1000,3) \\ &\tilde{P}_3(s) := P_{app}(s;3000,3) \\ &\Omega_1 = [1,5],\ (a_1,b_1,c_1) = (10,-1,0) \\ &\Omega_2 = [500,1100],\ (a_2,b_2,c_2) = (0,1,-2) \\ &\Omega_3 = [2000,8000],\ (a_3,b_3,c_3) = (-1.5,1,\kappa). \end{aligned} \tag{15}$$

As a result, we obtained $k_{\rm P} = 0.0499$, $k_{\rm I} = 4.6150$ and $\kappa = 0.3486$. Fig. 10 shows Nyquist plots of $L_\infty(s)$ and $L_{\{2,3\}}(s)$ for the compensator obtained here and these are drawn by a solid and broken line, respectively. In this figure, : and $*$ denote the ranges Ω_2 and Ω_3. From the figure, we can see that the maximization of the stability margin is achieved for the system without being too conservative. Also, we do not need the high-order model, meaning we can execute the loop shaping without increasing the computational loads.

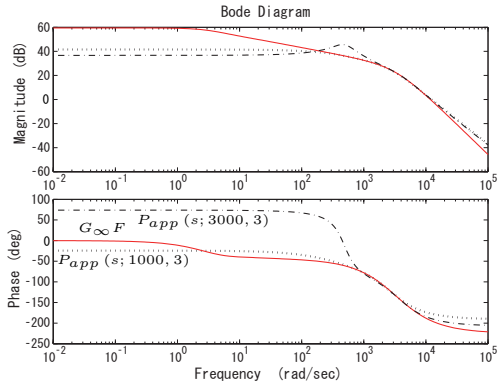

Fig. 9. Approximation via Taylor expansion

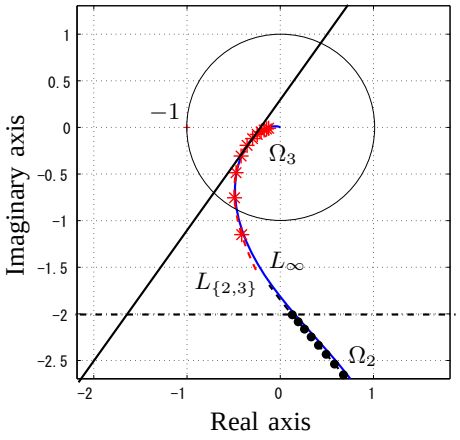

Fig. 10. Nyquist plot of the loop transfer functions

B. Consideration of the proposed technique for the actual machine

In this section, we consider the proposed technique for the actual machine. We minimize κ with several values of γ, which expresses the constraint shown by the chain line in Fig. 10, under the condition that for the loop transfer functions $\tilde{P}_i(s)$ $(i = 1,2,3)$ same as in (15), $k_{\rm P}$ and $k_{\rm I}$ satisfy the constraints

$$\begin{aligned} &\Omega_1 = [1,5],\ (a_1,b_1,c_1) = (10,-1,0) \\ &\Omega_2 = [100,500],\ (a_2,b_2,c_2) = (0,1,-\gamma) \\ &\Omega_3 = [2000,8000],\ (a_3,b_3,c_3) = (-1,1,\kappa). \end{aligned}$$

As a result, we obtained $k_{\rm P} = 9.6\times10^{-4}$, $k_{\rm I} = 7.3\times10^{-1}$ and $\kappa = 4.8\times10^{-3}$ when $\gamma = 0.1$ and $k_{\rm P} = 1.9\times10^{-3}$, $k_{\rm I} = 1.5$ and $\kappa = 9.6\times10^{-3}$ when $\gamma = 0.2$.

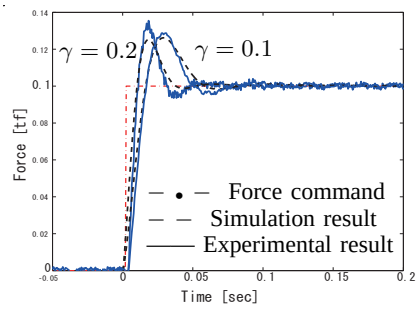

Fig. 11. Numerical simulation and Experimental result

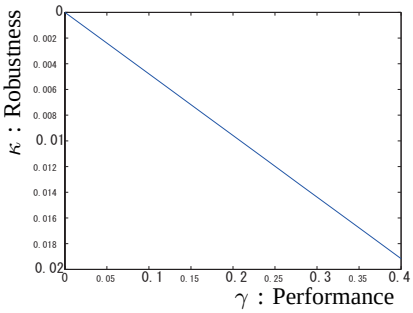

Fig. 12. Trade-off relation between κ and γ

Fig. 11 shows numerical simulations and experimental results for the obtained controllers. We can see from this figure that both numerical simulations and the experimental results converge to the target value and also that the convergence rate improves as the value of γ is larger. However, discrepancies of the system behaviors between the numerical simulation and the experimental result became larger along with enlarging γ. Furthermore, we could not execute the experiment over $\gamma = 0.3$ due to an oscillation of the actual machine. The reason why the oscillation occurs can be explained by the effect of uncertain elements, which were not considered in the modeling, causing a lack of robustness caused by too high gain.

In addition, we can see from Fig. 12 that a trade-off relation exists between γ and κ, i.e., guarantee of the gain in middle-frequency range and the robustness of the closed system. That is to say, we cannot improve the convergence rate without losing some of the stability margin. At the same time, we confirmed the fact from the experiment that the numerical simulations conformed to the experimental results if κ is obtained below about 0.01. Consequently, we can conclude that it is difficult to suppress the overshoot while keeping the convergence rate equal to that of Fig. 11 by tunings of the PI controller. In other words, we can theoretically show the performance limitation of the PI controller for the system by the proposed technique.

V. Conclusion

Spatially-distributed phenomena are important to industrial applications, while mathematical treatment of them are complex. In this paper, we derived an expression of the system as PDEs from the basic laws of physics and then analytically characterized the properties of the system in the frequency domain. From the analysis, we made clear that the essential structure of the system was identical to that of heat diffusion systems. Also, we derived the new model, which was suitable to control system design, in the frequency domain and proposed a new loop shaping technique via applying GKYP lemma. Consequently, we theoretically showed the performance limitation, which is hard to determine by heuristic tuning of the controller.

In addition, the model derived in section IV-A properly captures the features of the system without increasing the computational loads. There, we modeled the system suitably for the control system design by using more than one model. It indicates that we might suitably be able to model such distributed parameter systems, which have the diffusion structure, without using fine spatial discretization. These systems appear in many domains [12], [13], [14], e.g., chemical reactions in biology or mathematical finances, therefore our future work will be to devise applicable modeling techniques for them.

References

[1] H. Morita, A. Kato, T. Yamamoto and T. Shibata: WO publication, WO2009/028488

[2] Y. Nozaka: *Industrial Control System and Control Apparatus*, CORONA PUBLISHING CO., LTD (1995)

[3] D. K. Cheng: *Field and Wave Electromagnetics Second Edition*, ADDISON-WESLEY PUBLISHING COMPANY (1992)

[4] L. Ljung: *SYSTEM IDENTIFICATION*: *Theory for the User*, PRENTICE HALL PTR (1987)

[5] D. S. Bernstein: *Matrix Mathematics – Theory, Facts, and Formulas with Application to Linear Systems Theory –*, PRINCETON UNIVERSITY PRESS (2005)

[6] R. Curtain and H. Zwart: *An Introduction to Infinite-Dimensional Control Theory*, Springer (1995)

[7] R. Curtain and K. Morris: "Transfer functions of distributed parameter systems: A tutorial" *Automatica* 45 1101-1116 (2009)

[8] R. Padhi and S. F. Ali: "An account of chronological developments in control of distributed parameter systems" *Annual Reviews in Control* 33, 59.68 (2009)

[9] N. Abe and A. Kojima: *Control in Time-delay and Distributed Parameter Systems*, CORONA PUBLISHING CO., LTD. (2007)

[10] H. Takami and T. Kawamura: *Partial Differential Equations by the Finite Difference Method*, University of Tokyo Press (1994).

[11] N. W. McLachlan: *Bessel Functions for Engineers Second Edition*, OXFORD UNIVERSITY PRESS (1955)

[12] J. Crank: *The Mathematics of Diffusion*, OXFORD UNIVERSITY PRESS (1973)

[13] W. M. Deen: *Analysis of Transport Phenomena*, OXFORD UNIVERSITY PRESS (1998)

[14] H. S. Carslaw and J. C. Jaeger: *Conduction of Heat in Solids*, OXFORD SCIENCE PUBLICATIONS (1986)

[15] M. Krstic and A. Smyshlyaev: *Boundary Control of PDEs – A Course on Backstepping Designs –*, Society for Industrial and Applied Mathematics Philadelphia (2007)

[16] T. Iwasaki and S. Hara: "Generalized KYP lemma: Unified frequency domain inequalities with design applications" IEEE Trans. Auto. Contr. , 50(1), pp. 41-59, (2005).

[17] P. Gahinet, A. Nemirovski, A. J. Laub and M. Chilali: *LMI Control Toolbox – For Use with MATLAB –*, The MATH WORKS Inc. (1995)